Article

Not peer-reviewed version

Exploring Cobalt Doping Methods for Enhancing Blue-TiO2 Catalyst Efficiency

Roberta Irodia , Camelia Ungureanu , Veronica Sătulu , Vasilica Mihaela Mîndroiu *

Posted Date: 11 July 2023

doi: 10.20944/preprints202307.0653.v1

Keywords: Nanostructures; Blue-TiO2 nanotubes; Antimicrobial; Antibiotics; Photocatalytic

Article

Exploring Cobalt Doping Methods for Enhancing Blue-TiO_2 Catalyst Efficiency

Roberta Irodia [1], Camelia Ungureanu [1], Veronica Sătulu [2] and Vasilica Mihaela Mîndroiu [1]*

[1] University POLITEHNICA of Bucharest, Faculty of Chemical Engineering and Biotechnologies, 1-7 Polizu, 011061, Bucharest, Romania

[2] National Institute for Laser, Plasma and Radiation Physics, Atomiștilor 409, Măgurele, RO-077125, Romania

* Correspondence: mihaela.mindroiu@upb.ro; Tel.: (+40-21-4023930)

Abstract: This study presents a straightforward electrochemical and plasma deposition method for producing Cobalt-doped Blue-TiO_2 nanotubes with enhanced catalytic properties. After a titanium plate has been anodized, specific procedures are carried out that cause oxygen vacancies to form inside the TiO_2 nanostructures. The obtained catalysts were subjected to electrochemical tests (to identify charge transfer resistance and flat band potential), optical analysis (to determine the band gap and Urbach energy) and also characterized in terms of morphology, wettability and antibacterial effect in order to understand and analyze the impact of the Co doping method on the final catalyst characteristics. A hydrophilic film with star-shaped structures and with antibacterial effect was created when cobalt was electrochemically doped to Blue-TiO_2 nanotubes. By using this electrochemical doping technique, the Urbach energy was raised from 1.171 to 3.836 eV while the band gap energy was decreased from 3.04 to 2.88 eV. Additionally, photodegradation experiments using artificial doxycycline (DOX) water were conducted to determine the practical relevance of the research findings. In areas like antimicrobial applications and photodegradation of DOX, these extra experiments aimed to show the practical applicability and potential advantages of the research findings.

Keywords: nanostructures; blue-TiO_2 nanotubes; antimicrobial; antibiotics; photocatalytic

1. Introduction

Worldwide is observed an increased vitamin, immune boosters, combination medications, or cocktails of antivirals, antibiotics, steroids, and antifungals antibiotics consumption but among of these, antibiotics are a major source of concern[1, 2]. Many organisms such as Salmonella, Pseudomonas Aeruginosa have developed resistance to tetracyclines (TCs) [3, 4], the second most widely used class of antibiotics in human and veterinary treatment because tetracycline is effectively eliminated in the urine by glomerular filtration. Doxycycline (DOX) is a semi-synthetic tetracycline antibiotic that has a prolonged effect and is effective against a wide range of bacteria [5, 6]. As literature reported [7-9], doxycycline has a significant role in the COVID-19 therapy also.

Salmonella, a bacterium often linked to foodborne illnesses, can also be present in water and wastewater if contaminated with fecal matter. It is crucial to treat residual water to eliminate pathogens [10, 11]. It's worth noting that although Salmonella can survive in water for a period, particularly in warmer temperatures, it typically requires a nutrient source for multiplication [12, 13]. Pseudomonas aeruginosa, a common bacterium found in water and soil [14], can pose significant concerns in residual waters or wastewater. It is known for its ability to survive in various environmental conditions and persist in water for extended periods [15-17]. Treating residual waters to eliminate Pseudomonas aeruginosa is difficult due to its resistance to many disinfection methods, including some antibiotics[18, 19]. Hence, it is imperative to develop technologies for the removal of organic compounds and bacteria from water.

Therefore, the emergence of water contamination elevated the importance of electrochemical technologies that involve chemical, physical, or biological stages. An example is represented by water depollution through procedures involving photocatalysis based on TiO_2 nanostructures. Titanium

 doi:10.20944/preprints202307.0653.v1

dioxide (TiO_2) a nontoxic material, due to its great chemical stability, high resistance to photo corrosion, and inexpensive cost, has been one of the most investigated materials in the past few years [20, 21]. TiO_2 photocatalysts most efficient and stable can be developed out of nanomaterials with morphologies ranging from 0D to 3D and among all these forms, TiO_2 nanotubes (NT) are a part of 1D titanium nanostructures and are remarkable nanostructured photocatalysts, in large part due to their exceptional electron transport capabilities [22]. While nanostructured TiO_2 possesses remarkable properties, it is not without its limitations. As a semiconductor, it exhibits a forbidden band in the energy bands where electronic transitions take place [23]. This band gap restricts TiO_2 to respond only to UV light irradiation. The key challenge in TiO_2 studies lies in progressively reducing the energy of the forbidden band to enable irradiation with visible light from the solar spectrum. Numerous research have been undertaken to improve the photocatalytic activity of TiO_2 by doping with a transition metal oxide such as Fe, Zn, Cu, Ni, Co and V [24]. Doping TiO_2 with these metals effectively reduces the band gap for photo-excitation (red shift) while also lowering the recombination rate of photogenerated electron-hole pairs [24]. Despite the extensive exploration of various dopants, a significant focus has been placed on investigating Co-doped TiO_2 thin films. These films have attracted considerable attention due to their ability to display ferromagnetic behavior under typical room temperature conditions. This characteristic makes them highly suitable for many applications. Additionally, Co-doped TiO_2 thin films also show promise in enhancing their photocatalytic properties within the visible region, opening up possibilities for efficient light-driven chemical reactions [25, 26]. In this study, we introduce a new photo-electro-catalyst designed for the TCs degradation from wastewater. Specifically, we present the utilization of blue TiO_2 nanotubes (BT) doped with Cobalt ions as a novel electrocatalyst. The fabrication process involves the creation of anatase TiO_2 nanotube arrays followed by cathodic polarization [27], which are then subjected to metal doping through either electrochemical techniques or plasma treatment. The resulting material exhibits remarkable characteristics, including stable and irreversible electrochromism as well as high conductivity.

This study aims to emphasize the dual functionality of the photocatalyst obtained in our research. The photocatalyst possesses the unique ability to serve a dual purpose: firstly, it can effectively eliminate pathogenic bacteria present in water, contributing to water purification efforts. Secondly, it exhibits photo-electro-catalytic properties, enabling the efficient degradation and removal of organic compounds from water. By showcasing the photocatalyst's versatile capabilities, this research highlights its potential in addressing both bacterial contamination and organic pollution in water sources.

2. Experimental

2.1. Doped catalysts preparation

2.2.1. Blue TiO_2 nanotubes electrochemically obtained on Titanium plate.

Blue titanium dioxide nanotubes **(BT)** were produced by anodizing recycled Titanium plates taken from aerospace industry (considered waste products from the production line) at 40 V for 2 hours in a two-electrode cell. The precursor electrolyte is composed of ethylene glycol (EG) (Sigma Aldrich), 10% (vol.) of water, and 0.3% (vol.) of ammonium fluoride (NH_4F) (Sigma Aldrich) (Solution 1). After anodization, the sample was submerged to calcination in an oven at 450° C for 2 h. After this step, the sample is activated and more stabilized in the same anodization precursor solution for 10 minutes at 4 V. As a final step, reduction is made in an EG solution which contains also H_2O_2 for 4 minutes at -40 V.

2.2.1. Cobalt doping of the blue TiO_2 nanotubes

To highlight the most efficient Cobalt (Co) doping method of BT previous obtained on titanium electrodes, two doping methods were applied: electrochemical technique and plasma treatment.

Preprints (www.preprints.org) | NOT PEER-REVIEWED | Posted: 11 July 2023 doi:10.20944/preprints202307.0653.v1

The pulsed chronoamperometry method was used for the electrochemical Co doping technique (see Figure 1), which involved immersing a BT plate into a specific Co solution and applying a potential domain (vs. Ag/AgCl) for 200 cycles, at room temperature, using a potentiostat/galvanostat from the Metrohm Autolab (PGSTAT 302N) system. The electrochemical Co doping / blue TiO_2 nanotubes **(BT/Co-E)** photocatalyst was obtained.

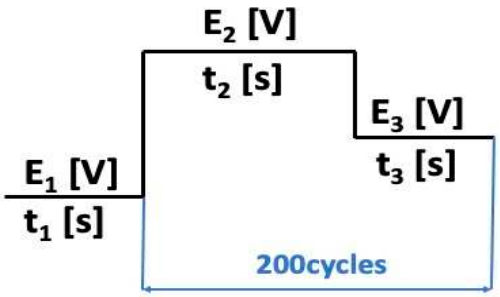

Figure 1. Pulsed chronoamperometry scheme used for Co electrodeposition on BT electrode.

were:

- E_1 is -1.5 V, t_1 = 2 s, initiation of cobalt nucleation takes place.
- E_2 is open circuit potential, and t_2 = 5 s.
- E_3 is -0.95 V, t_3 = 5 s, cobalt deposition takes place

Co solution was obtained according with literature[28]. A molecular ratio of Co $(NO_3)_2$: HNO_3 = 1:1 was used to obtain an aqueous solution of Co $(NO_3)_2$.

The plasma Co doping / blue TiO_2 nanotubes (BT/Co-P) sample was obtained by deposited Cobalt using plasma magnetron sputtering method onto BT plate support. We used a magnetron plasma source, with 1 inch Co target (99,9% from Kurt Lesker Company) and RF power supply generator to generate plasma. Details about experimental plasma set-up descriptions are presented in our previously report [29]. In the present work we use the following parameters: RF power supply of 100 W, a basic pressure at about 4×10^{-5} mbar (without gases) and a working pressure 5×10^{-4} mbar for 100 sccm of Ar. The deposition time of Co was 30 seconds.

For an easy understanding of the work stages, the steps involved are shown in next figure:

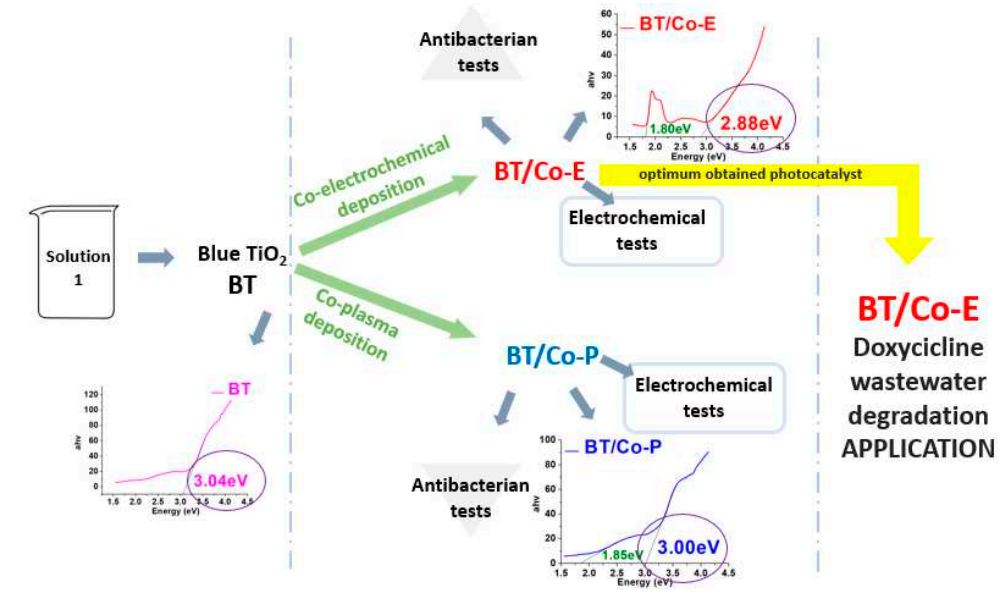

Figure 2. A description of the steps taken to create a photocatalyst with improved properties.

 doi:10.20944/preprints202307.0653.v1

2.1. Catalysts characterization and applicability

To study the *morphological characteristics* of obtained catalysts, SEM and EDX were performed using Scanning Electron Microscope including Oxford EDX detector-analyser.

Optical characteristics were performed using Perkin Elmer Lambda 650-850-950 UV-Vis spectrophotometer.

Wettability. The sessile drop method was used along with an optical contact angle meter (Contact Angle Meter – KSV Instruments CAM 100) fitted with a camera to determine the contact angles of distilled water solvent onto samples.

Electrochemical methods as by Electrochemical Impedance Spectroscopy (EIS) and Mott Schottky were performed to investigate the interfacial charge-separation efficiencies of prepared photocatalysts, using potentiostat/galvanostat from the Metrohm Autolab (PGSTAT 302N) system.

Antibacterial behaviour. The effectiveness of the materials' antibacterial properties was measured against two different harmful microbial strains Salmonella typhimurium - ATCC 14028 and Pseudomonas aeruginosa - ATCC 15442. Luria Bertani Agar (LBA) plates were used for bacterial culture [30]. The LBA compositions are peptone (Merck), 10 g/L; yeast extract (Biolife) 5 g/L, NaCl (Sigma-Aldrich) 5 g/L and agar (Fluka) 20 g/L. The stock of bacterial culture was kept at 4 °C.

Percentage of growth inhibition (I%) was used to assess antibacterial efficacy.

$$I\% = [(B_{18} - B_0) - (C_{18} - C_0)]/(B_{18} - B_0) \times 100 \quad (1)$$

where "I" is the rate of growth inhibition, B18 - blank - compensated optical density (OD) at 600 nm, B_0 - blank-compensated OD600 of the positive control organism at 0 h, C_{18} - negative control-compensated OD600 of the organism in the presence of test sample at 18 h, and C_0 - negative control-compensated OD600 of the organism in the presence of test sample at 0 h.

Sterilized samples were incubated in a Laboshake Gerhardt shaker for 18 hours at 37 °C and 250 rpm in 10 mL of Luria-Bertani broth (the sterile medium was inoculated with 1% bacteria). To determine bacterial proliferation, the optical density of the samples and the control (bacteria culture without sample) was measured at 600 nm using a UV-VIS spectrophotometer (Jenway Spectrophotometer).

Photodegradation applicability. DOX (hydrochloride salt, MW = 480.9 g mol^{-1}) was purchased from DELOS Medica. As found in literature [31], the antibiotic changes into different species based on the pH. These species are $DXCH^{3+}$ at pH 9, $DXCH^{2\pm}$ at pH 6, $DXCH^{-}$. Moreover, 70% of the molecule at pH 3 is $DXCH^{3+}$, 98% of the molecule at pH 6 is $DXCH^{2\pm}$, and 75% of the molecule at pH 9 is $DXCH^{-}$ [31].

DOX photodegradation was carried out in a quartz cell enclosed in a faradaic cage where outside light could not penetrate. Mercury vapor lamps fitted with filters from 200-600 nm wavelengths were utilized as illumination, illuminating the sample from one side of the reaction cell at around 5 cm. A D Lab MS-PA magnetic stirrer was used to control the stirring of the fluid. With NaOH and/or HCl solutions, the solution's pH was adjusted to the desired value. Prior to irradiation, 10 mL of a known concentration DOX solution was added in the cell, and the stirring was turned on. Before being exposed to light, the photocatalyst electrodes were immersed in DOX solution for 30 minutes to achieve optimal DOX adsorption at the solid's surface. A fixed volume of solution was exposed to light for various periods.

All the characterizations and tests were run in triplicate for maximum reproducibility.

3. Results

3.1. Characterization of the synthesized electrodes

Physicochemical characterisation of BT, BT/Co-E and BT-Co-P electrodes by SEM, EDX and wettability

In Figure 3b) after anodized process the TiO_2 electrode is observed white, but turns into a black colour for 5 seconds after annealing at 450° C and after cathodic polarization it is stabilized to a blue colour (obtained stable BT electrode) caused by electrochromism [32]. In fact, the electrochromic

Preprints (www.preprints.org) | NOT PEER-REVIEWED | Posted: 11 July 2023 doi:10.20944/preprints202307.0653.v1

effect is caused by the change from Ti^{4+} to Ti^{3+} and the intercalation of protons. The network structure of BT film was well organized, and a thickening of the tubular walls is observed with the outer diameter of the nanotubes of 100 nm approximately (see Figure 3a). Through reduction, the concept of self-doping was developed.

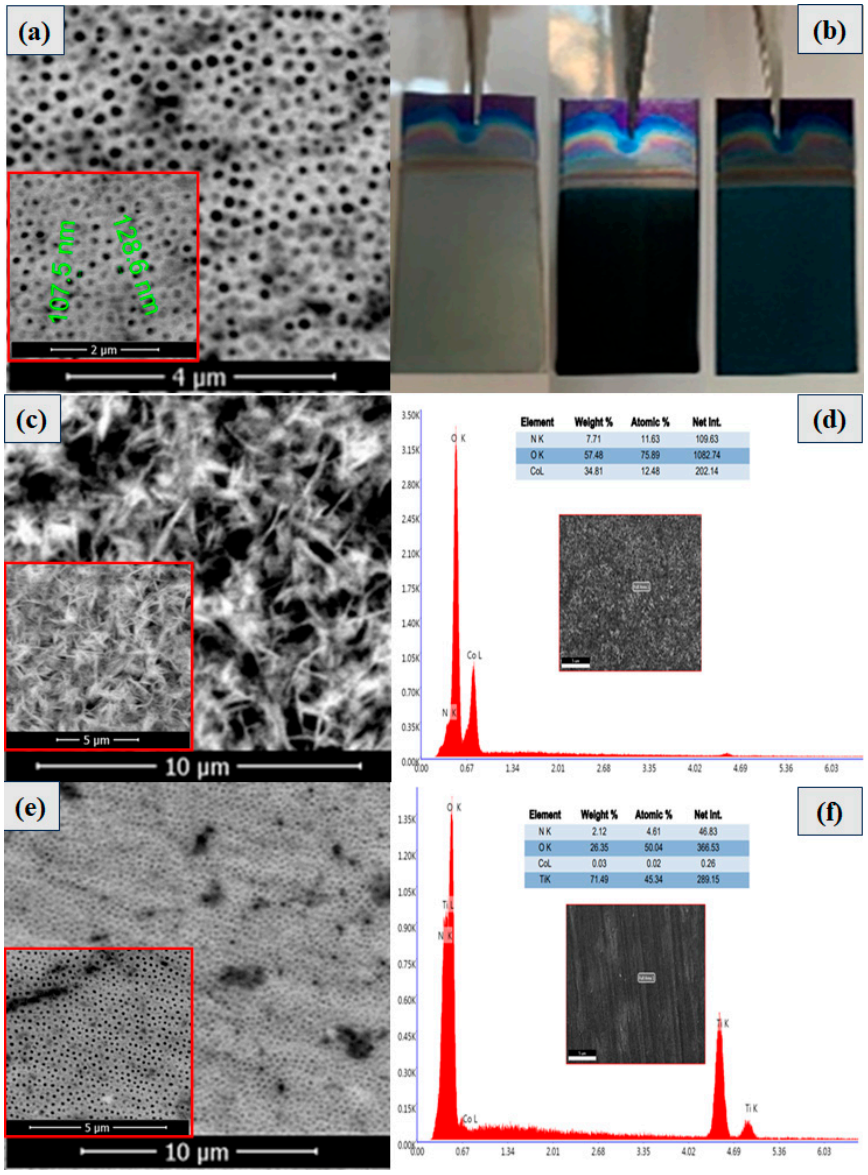

Figure 3. SEM images recorded at various magnifications for (a) BT; (c) BT/Co-E; (e) BT/Co-P. (b) Digital photos of BT surface after anodization, annealing and reduction. EDX spectra for (d) BT/Co-E and (f) BT/Co-P.

Following the metal doping, SEM images (Figures 3c and 3e, respectively) were captured at different magnifications to examine various structures. The presence of cobalt is highlighted by the formation of star-shaped nanostructures electrochemically doped with cobalt (BT/Co-E), according to Figure 3c). Co was electrochemically deposited onto the BT surface and completely doped it. The results of the EDX test, which show that there is approximately 34.81% cobalt in the BT nanostructure, also support the presence of cobalt there.

Furthermore, metal doping was accomplished using plasma technique. As a result, the SEM images for the BT/Co-P sample are displayed below (Figure 3e)). In contrast to the previously discussed sample (BT/Co-E), there is no apparition of the formation of Co star-shaped structures. There is no observable morphological change also from the BT substrate after Co doping in the plasma has been accomplished (see Figure 3a, and 3e). Also, EDX results for the BT/Co-P sample showed a small amount of cobalt (Figure 3f)) of about 0.03%.

Preprints (www.preprints.org) | NOT PEER-REVIEWED | Posted: 11 July 2023 doi:10.20944/preprints202307.0653.v1

Contact angle analysis was used to investigate the wettability property of the samples. The outcomes are shown in Table 1 and it can be observed that BT/Co-E had a minimal contact angle. As the data show, Co doping was shown to be more effective at decreasing the contact angle. The hydrophilicity of these photocatalysts was confirmed by reducing the contact angle of surfaces with Co-doped Blue TiO_2 compared to BT, which is an important metric for antibacterial behaviour. The higher the antibacterial action, the lower the contact angle [26].

Table 1. Contact angle measurements.

Sample	Contact angle (°) Water solvent
BT	30 ± 0.13
BT/Co-P	10 ± 0.04
BT/Co-E	6 ± 0.05

Optical parameters - Band gap energy and Urbach energy.

As literature reported, TiO_2's high band gap (approximately 3.2 eV in the anatase phase) limits its absorption to the solar spectrum's ultraviolet rays, making titania powders unsuitable for use as a visible light absorber [33].

As a result, the goal is to reduce the band gap, which in this case is reduced from 3.04 eV for BT to 2.88 eV and 3 eV for BT films doped with cobalt via electrochemical and plasma methods, respectively. TiO_2's band gap was calculated by Tauc plot representing $\alpha h\nu$ vs energy [34], were E_g is the band-gap energy, $h\nu$ is the energy of the incident photon and α is the absorption coefficient [35]. The introduction of some localized defect states into the band gap of Blue TiO_2 by cobalt doping process is what causes the reduction of band gap in case of doped BT catalysts.

The Urbach tail, with an associated Urbach energy, is responsible for the absorption tail produced by these localized defect states, that extends far into the forbidden gap [36]. The Urbach energy was calculated from the absorption spectrum using the formulas below [37]:

$$\alpha = \alpha_0 . exp\left(\frac{h\upsilon}{E_u}\right) \text{ and } E_u = \left(\frac{d[\alpha h\upsilon]}{d[h\upsilon]}\right)^{-1} \quad (2)$$

here α_0 is a constant and E_u is the Urbach energy.

The Urbach energy was calculated as E_u = 1/Slope, which is the inverse of the linear region beneath the band gap slope, from the graph ln(α) = f (photon energy) (Figure 4b). It is evident from the above properties of the developed BT nanostructures electrochemically doped with Cobalt exhibits the performance features required for further photocatalysis applications. As shown in Figure 4b, the Urbach energy increased from 1.171 eV to 3.836 eV, indicating that the BT/Co-E electrode has more structural defects than BT. According to the EDX results (Figure 3d), a higher concentration of Co was doped using an electrochemical method, increasing absorption at longer wavelengths, and reducing bandgap.

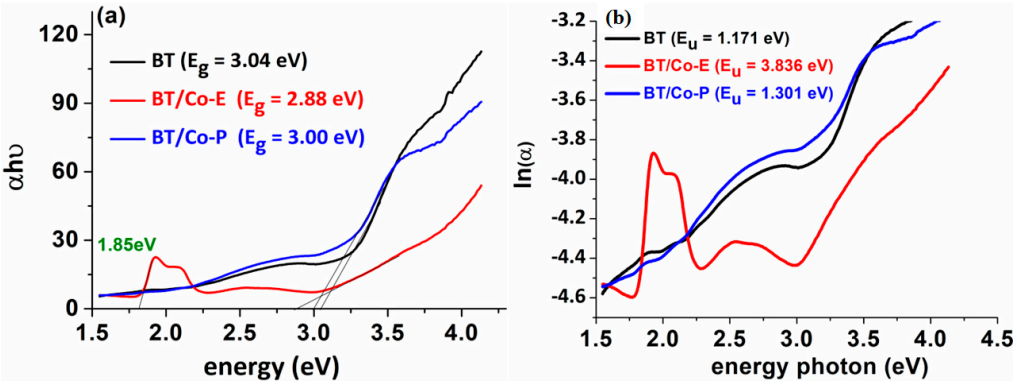

Figure 4. (a) Represented band-gap energy found from Tauc plot; and (b) ln(α) versus photon energy plots for Urbach energy determination.

Preprints (www.preprints.org) | NOT PEER-REVIEWED | Posted: 11 July 2023 doi:10.20944/preprints202307.0653.v1

Antibacterial tests

In continuous, as-prepared Co-doped TiO_2 nanostructures were tested for their antibacterial activity against Salmonella and Pseudomonas aeruginosa. Previous reported literature studies found antibacterial action on TiO_2 nanotubes, but it was certainly unsatisfactory for use as an antibacterial surface when compared to other studied modified surfaces [38].

The developed photocatalysts' antibacterial activity were displayed in Figure 5. The outcomes of the antibacterial tests indicate that Co-doped TiO_2 blue nanotubes are highly effective against both Gram-negative and Gram-positive bacteria compared to undoped BT. According to the EDX results, the concentration of Co in the doped samples seems to have not an visible effect on the antibacterial activity. Even so, BT/Co-E has the most effective antibacterial action.

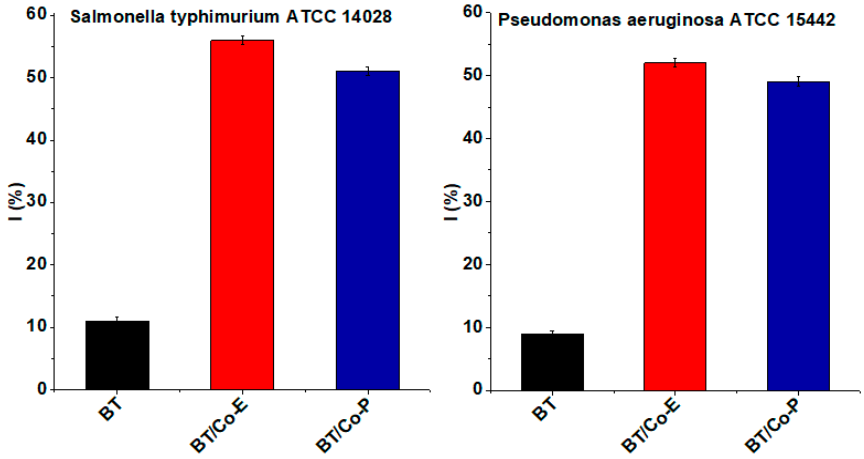

Figure 5. Antibacterial efficiency charts of the obtained samples against Salmonella typhimurium and Pseudomonas aeruginosa.

Electrochemical features of the developed electrodes

Electrochemical impedance spectroscopy (EIS) and Mott Schottky (MS) were used to estimate the charge transfer and recombination process at the electrode/electrolyte interface. The EIS measurements for BT, BT/Co-E, and BT/Co-P are done at free potential in 0.9% NaCl solution and in the frequency domain between 0.01 and 10,000 Hz with an amplitude of ± 10 mV. The Nyquist plots for these measurements are shown in Figure 6(a). A Randles equivalent circuit, depicted in the inset of Figure 6a, was proposed to understand electrode behaviour by associating the arc radius with the charge transfer resistance (R_{ct}) at the obtained catalyst / NaCl solution interface, which is in parallel with a constant phase element (CPE). R_{ct} values for BT, BT/Co-E and BT/Co-P were determinate as 370 kΩ, 76 kΩ and 143 kΩ respectively. The BT/Co-E film with the lowest R_{ct} value has the highest interfacial charge transfer efficiency and the slowest recombination rate, which is an important factor to consider in catalytic degradation applicability.

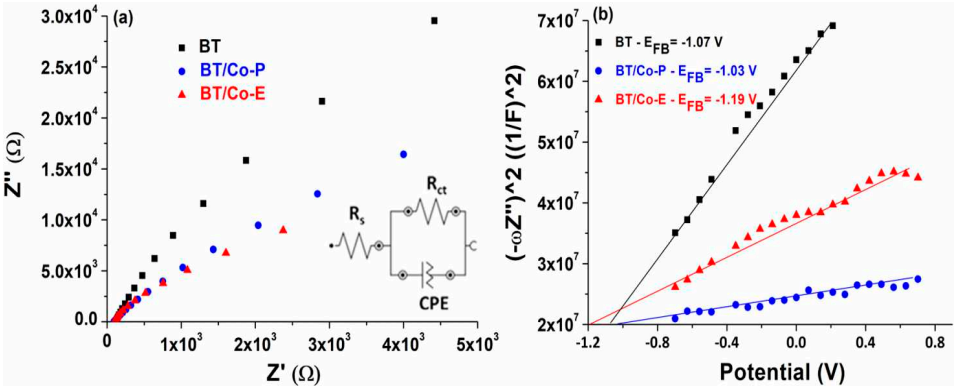

Figure 6. (a) Nyquist plots and (b) MS plots.

Preprints (www.preprints.org) | NOT PEER-REVIEWED | Posted: 11 July 2023 doi:10.20944/preprints202307.0653.v1

The impedance data was analysed using the Mott-Schottky equation (3), which is defined as follows:

$$\frac{1}{C^2} = \left(\frac{2}{q\varepsilon\varepsilon_0 N_D}\right)\left(E - E_{fb} - \frac{kT}{q}\right) \quad (3)$$

where C is capacity of the space charge layer, q – elementary charge, ε_0 - vacuum permittivity, ε - dielectric constant, N_D –concentration of donors, E – applied external bias, E_{fb} – flat band potential, k – Boltzmann's constant, T- absolute temperature.

The slope of the Mott-Schottky plot reveals the doping level (N_D), and the flat band potential (E_{fb}) is calculated by extrapolating to $1/C^2 = 0$, which depends on the recombination rate and interfacial charge transfer [34].

In contrast to normal TiO_2, which has a positive slope [39], all Mott-Schottky plots for doped and undoped blue TiO_2 have a negative slope. This is because the TiO_2 conductivity is changed from n-type to p-type due to the application of reduction and Co-doping procedures, resulting in greater charge mobility [40].

The calculated E_{fb} for BT is -1.07 V and -1.03 V for BT/Co-P, which are close values due to a small amount of Co doped by the plasma method, according to the EXD results (Figure 3f). In the case of BT/Co-E obtained through electrochemical doping of BT with Cobalt, E_{fb} is shifted to a more negative potential of -1.19 V, due to more localized defect states associated with higer Urbach energy. As a result, the electrochemical doping method improves the photocatalytic abilities of the BT/Co-E surface, implying a slower recombination rate, which is in accordance with the decrease in charge transfer resistance determined by EIS [41].

The flat band potential values obtained from Mott-Schottky plots are commonly regarded as the conduction band potential (CB) for semiconductors [39].

Correlating with the variations in Urbach energy (Figure 4b) is a change in the doping level (N_D) of BT, BT/Co-E, and BT/Co-P from 1.32×10^{21} cm^3 to 1.23×10^{22} cm^3 and 2.77×10^{21} cm^3. After electrochemical doping with a greater quantity of Cobalt (according to EDX results from Figure 3d), the flat band potential of BT shifts to more negative values. This suggests that the BT/Co-E film has better photocatalytic properties and a higher doping level, because of improved charge transfer efficiency in bulk and at the electrode / electrolyte interface [40].

Finally, the BT/Co-E catalyst obtained through electrochemical Co doping of BT has the highest interfacial charge transfer efficiency and the slowest recombination rate, as well as better p-type conductivity than the BT/Co-P catalyst obtained through plasma doping. These properties are due to the presence of more localized defect states caused by a higher amount of Cobalt star-shaped nanostructures electrochemically doped onto BT, which increases absorption at longer wavelengths and decreases bandgap while also improving wettability and increasing antibacterial effect.

Figure 7 depicts the schematic energy-level diagram for the investigated catalysts based on the MS E_{fb} results (Figure 6b) and UV-VIS E_g data (Figure 4a).

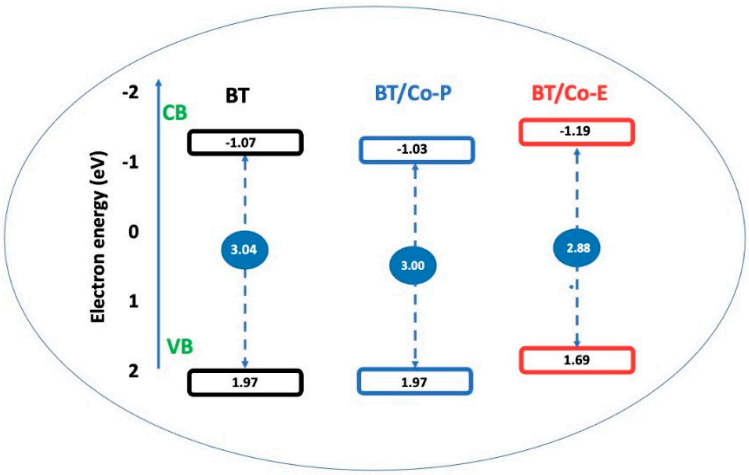

Preprints (www.preprints.org) | NOT PEER-REVIEWED | Posted: 11 July 2023 doi:10.20944/preprints202307.0653.v1

Figure 7. Schematic energy–level diagram of the BT, BT/Co-P and BT/Co-E photoelectrodes.

The measured CB and E_g were used to calculate the valence band (VB) energies.

The BT/Co-P catalyst has the same VB value (1.97 eV) as BT, indicating that plasma doping does not significantly change the catalytic properties of BT, as previously shown by surface and electrochemical data. The BT film electrochemically doped with Co, on the other hand, has the narrowest bandgap energy of all the catalysts studied and VB is reduced by 0.62 eV, indicating that Co has been doped in an adequate amount and that the structure, optical, and electrochemical characteristics have been enhanced. This makes the BT/Co-E catalyst the best candidate among all investigated catalysts for using in DOX photodegradation.

3.2. Applicability of the BT/Co-E catalyst

Influence of pH on the photocatalytic degradation of DOX. Figure 8 displays the variations in UV-Vis spectra of a DOX solution throughout a standard photodegradation experiment carried out at diferrent pH values, 2.5, 5.5 respectively 9.5. In presence of BT/Co-E catalyst, the DOX solution shows a spectrum with two maxima observed at 271 nm and 375 nm [31]. Depending on the chosen pH, the DOX solution shows different colors. At an acidic pH no coloration of the solution is observed, at a pH of 5.5 the solution becomes slightly yellow and at a pH of 9.5 the solution becomes slightly pink, as it was observed also in other studies from literature [31].

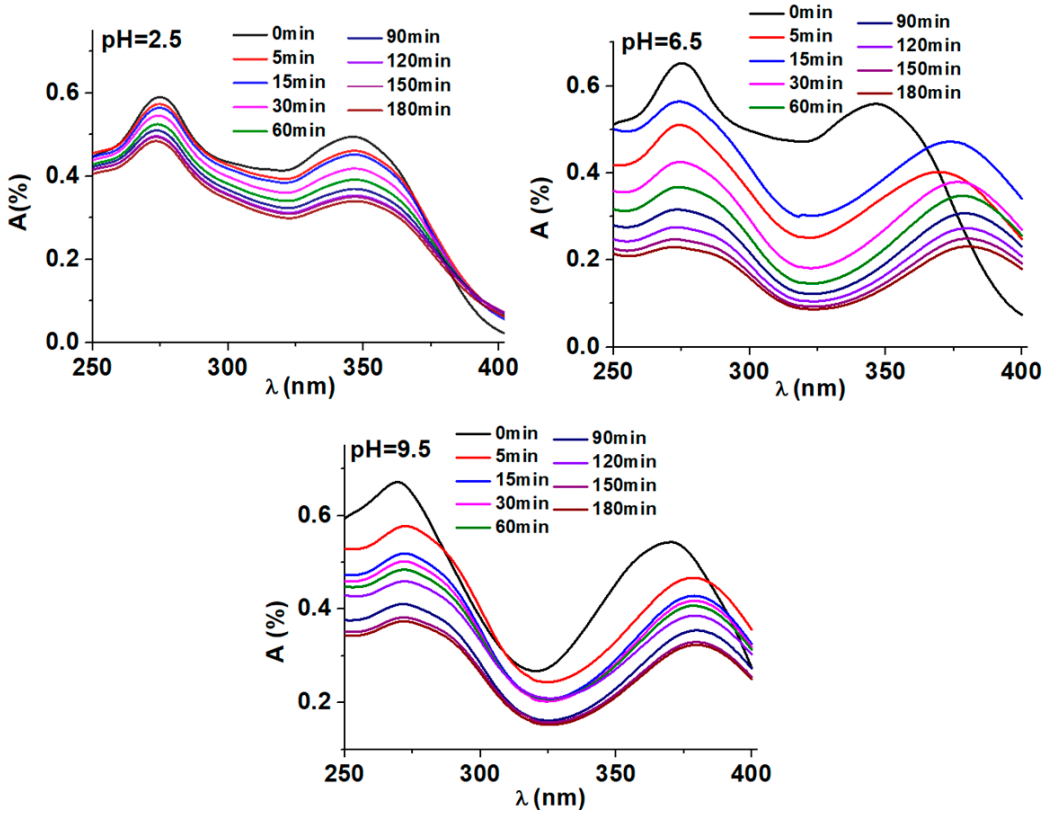

Figure 8. Evolution of UV-Vis Spectra in the DOX solution during varied reaction times in pH-controlled photodegradation experiments.

It is significant to note that even after many hours of exposure, the absorbance at any wavelength never stabilizes, indicating that complete photo-degradation was not accomplished. Under the conditions of our experiment, the findings indicate that the photodegradation of DOX is quite distant from reaching equilibrium. Furthermore, these findings reveal that photodegradation and the mechanism are very pH dependent. Better results when exposing the catalyst to light are observed at a pH of 6.5, so compared to the other degradations at the other pHs, the absorption reduces significantly.

Preprints (www.preprints.org) | NOT PEER-REVIEWED | Posted: 11 July 2023 doi:10.20944/preprints202307.0653.v1

Photo-electro-catalytic application. Going forward with our studies, it may be deduced from the pH influence graphs that the best outcomes are obtained at a pH of 6.5. As a result, for further testing, a 6 mol/L DOX solution with a pH of 6.5 will be utilized. Both photodegradation and photoelectrodegradation tests were conducted in order to create a dual system in which DOX degradation from water occurs. An efficient and cost-effective system is characterized by the synergic combination between light and a photocatalyst to generate reactive oxygen species (ROS). These reactive oxygen species are responsible for breaking down the organic compound.

The efficiency of photodegradation and photoelectrodegradation will be compared here. The DOX solution was photoelectrocatalytically degraded at three distinct potentials: 0.35 V, 0.50 V and 0.80 V, in order to demonstrate the impact of input potential on DOX degradation efficiency. According to recent research in the literature [42] the oxidation potential of TCs is founded at almost 0.80 V, although as shown in the data below (Figure 9b), the degradation of DOX has a poor response to this potential. The oxidation potential value of DOX was drastically reduced to 0.35 V due to BT/Co-E with enhanced catalytic features so this is why three additional imposed potentials were chosen.

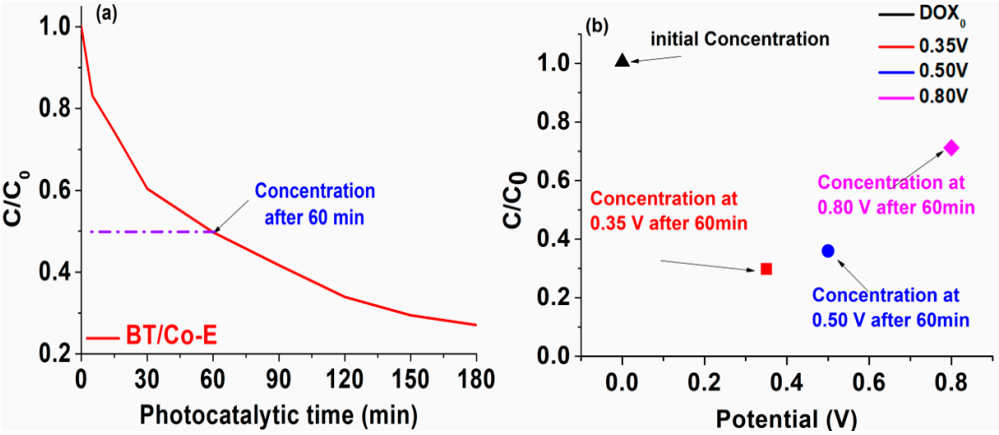

Figure 9. (a) Photocatalytic and (b) Photo-electro-catalytic DOX degradation efficiency.

After only 60 minutes, the photo-electro-catalytic system reaches 70% degradation efficiency, as can be seen in Figure 9b. An efficiency of 50% degradation is attained after 60 minutes in the photocatalytic system (Figure 9a). Given that the photocatalysis investigations were conducted over a period of 180 minutes, it was found that the degradation reached 80% efficiency, but only after irradiating for a triple time compared to the time allocated to the photoelectrodegradation.

It was clearly observed that the system doesn't work as well only when exposed to UV-Vis light, so the system will be coupled up to a potentiostat once the 60 minutes of photodegradation process is done. This potentiostat will apply a potential of 0.35 V, effectively fast eliminating the compounds that have resulted from the photocatalytic degradation and which were not previously degraded. This could be because when exposed to light, the electron-hole pairs generated by the photons were quickly separated. This separation resulted in a significant number of electrons being produced, which facilitated the transfer of electrons through the electrode. As a result, the photocurrent, which is the current generated by light, showed a rapid improvement upon the onset of light exposure. Eventually, the photocurrent reached a stable state after continuous exposure to light.

The degradation kinetics was calculated for the photocatalytic degradation using the Langmuir–Hinshelwood pseudo first-order kinetic model [43], which is shown in the equation below, was used to study the speed of the process.

$$Ln\left(\frac{C}{C_0}\right) = k \times t \quad (4)$$

where C_0 and C are the initial concentration (mol/L) and final concentration (mol/L) of DOX and t (min) and k (min^{-1}) are the solution concentration and the rate constant.

Preprints (www.preprints.org) | NOT PEER-REVIEWED | Posted: 11 July 2023 doi:10.20944/preprints202307.0653.v1

Figure 10 shows that for DOX degradation in the presence of BT/Co-E catalyst and UV-Vis light, the relationship between $Ln\left(\frac{C}{C_0}\right)$ time (min) is linear. The R^2 values for the association coefficients were greater than 0.900, and the first-order kinetic model did a good job of fitting the experimental data. Looking closely at the degradation diagram, two distinct degradation tendencies can be seen. Based on the slope of the linear plots, the first-order rate constants (k) were found to be 15×10^{-3} min^{-1} for the first degradation tendency and 0.5×10^{-2} min^{-1} for the second degradation tendency [44].

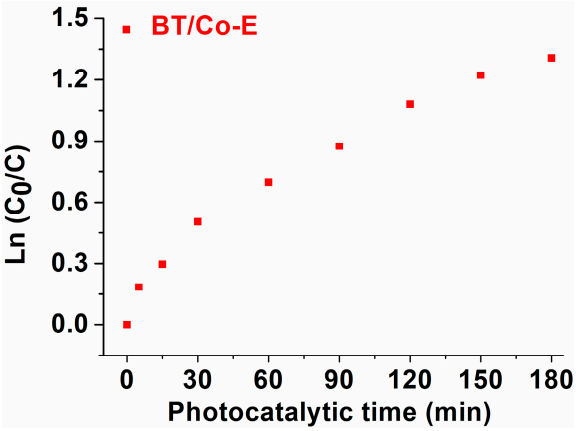

Figure 10. Photodegradation kinetics curve of DOX, pH=6.5.

Proposed mechanism of DOX degradation in the presence of BT/Co-E

Figure 11 shows a probable mechanism of BT/Co-E for DOX degradation based on the above characterization and photocatalytic activity results. The improved photocatalytic performance of TiO_2 could be explained as follows. Under visible-light irradiation, a Ti-O-Co hybridization energy level is formed, leading to a reduction in the bandgap. This reduction enhances the ability to excite electrons [45]. As the catalytic process unfolds, a small quantity of dissolved O_2 from wastewater reacts with the electrons generated by light, electrons produced by the CB of **Co-E** that were caught and transported to TiO_2 (**BT**), resulting in the production of a limited amount of O_2^{-}•radicals. This process will improve the electronhole separation efficiency.

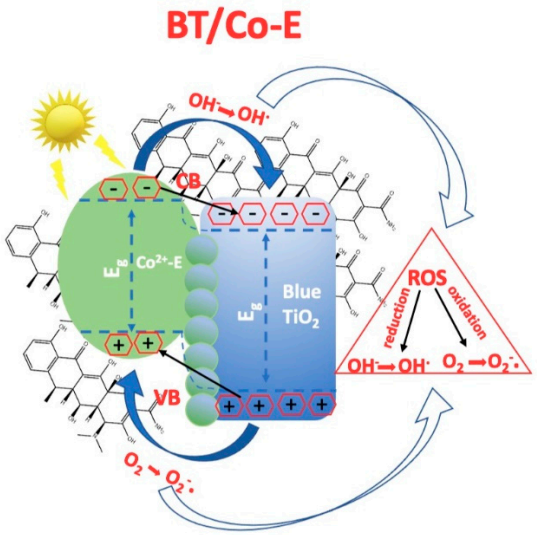

Figure 11. The mechanism of BT/Co-E photocatalyst.

Furthermore, a limited quantity of holes generated by light, situated in the VB, engage with water to produce·OH and $OH^{\cdot}$ Moreover, the holes existing in the VB of the doped photocatalyst will be stimulated in the presence of light and will transform water into hydroxyl-type compounds/hydroxyl radicals that will produce photocatalytic degradation.

4. Conclusion

By using electrochemical pulsed deposition and plasma magnetron sputtering, Co-doped Blue-TiO_2 samples were synthesized successfully. The results showed that doping blue-TiO_2 with star-shaped Cobalt deposited electrochemically gave the best results compared to doping blue-TiO_2 with Cobalt plasma magnetron sputtering, because has the highest interfacial charge transfer efficiency, the slowest recombination rate, and better p-type conductivity. Also the Urbach energy increased from 1.171 to 3.836 eV while the band gap energy decreased from 3.04 to 2.88 eV making this material an effective catalyst for a variety of applications, including photocatalysis, photo-electrocatalysis, water splitting, solar cells, the development of smart windows, batteries, etc.

The catalysts were also studied as antibacterial surfaces. Among the three photocatalysts obtained for this study, electrochemically doped blue-TiO_2 (BT/Co-E) has the strongest antibacterial effect. This indicates that this catalyt will eradicate antibiotic-resistant bacteria from wastewater.

All of these tests performed in this study, such as electrochemical, optical and antibacterial showed enhanced results for BT/Co-E doped and this sample was employed to photodegradation and photoelectrodegradation processes. In both cases, the effects of the degradation were satisfactory. With the photocatalytic system, 50% DOX was degraded after 60 minutes, and 80% DOX was degraded after 180 minutes. After 60 minutes of using the photoelectrocatalytic irradiation device, 70% yield was reached. The synergistic combination of light and applied potential makes the suggested system extremely straightforward, efficient, cost-effective and suitable for many other applications.

Author Contributions: Conceptualization, R. Irodia, V. M. Mîndroiu; Data curation, R. Irodia, V. M. Mîndroiu; Formal analysis, R. Irodia, C. Ungureanu, V. Sătulu, V. M. Mîndroiu; Investigation, R. Irodia, C. Ungureanu V. Sătulu, V. M. Mîndroiu; Methodology, R. Irodia, V. M. Mîndroiu; Resources, R. Irodia, C. Ungureanu, V. Sătulu, V. M. Mîndroiu; Writing—original draft, R. Irodia, V. M. Mîndroiu; Writing—review & editing, R. Irodia, V. M. Mîndroiu; The published version of the manuscript has been read and approved by all authors.

Funding: This work was supported by the following grant agreements: a grant of the European Social Fund from the Sectoral Operational Program Human Capital 2014-2020, through the Financial Agreement with the title "Training of PhD students and postdoctoral researchers in order to acquire applied research skills - SMART", Contract no. 13530/16.06.2022 - SMIS code: 153734.; and a grant of the Ministry of Research, Innovation and Digitization, CNCS - UEFISCDI, project number PN-III-P1-1.1-TE-2021-0417, within PNCDI III.

Institutional Review Board Statement: Not applicable

Informed Consent Statement: Not applicable.

Data Availability Statement: The raw/processed data generated in this work are available upon request from the corresponding author.

Acknowledgments: We acknowledge to Dr. Biță Bogdan from INFLPR-National Institute for Laser, Plasma and Radiation Physics, Măgurele, Romania, for EDX investigations. PhD student R. Irodia acknowledge for grant of the European Social Fund from the Sectoral Operational Program Human Capital 2014-2020, through the Financial Agreement with the title "Training of PhD students and postdoctoral researchers in order to acquire applied research skills - SMART". PhD student R. Irodia and Prof. V. M. Mîndroiu acknowledge the support from the grant of the Ministry of Research, Innovation and Digitization, CNCS - UEFISCDI, project number PN-III-P1-1.1-TE-2021-0417, within PNCDI III.

Conflicts of Interest: The authors declare that they do not have any known competing financial interests or personal connections that could appear to have influenced the work presented in this study.

References

1. Kutuzova, A.; Dontsova, T.; Kwapinski, W., Application of TiO2-Based Photocatalysts to Antibiotics Degradation: Cases of Sulfamethoxazole, Trimethoprim and Ciprofloxacin. *Catalysts* **2021,** 11, (6), 728.
2. Vaughn, V. M.; Gandhi, T. N.; Petty, L. A.; Patel, P. K.; Prescott, H. C.; Malani, A. N.; Ratz, D.; McLaughlin, E.; Chopra, V.; Flanders, S. A., Empiric antibacterial therapy and community-onset bacterial coinfection in patients hospitalized with coronavirus disease 2019 (COVID-19): a multi-hospital cohort study. *Clinical Infectious Diseases* **2021,** 72, (10), e533-e541.
3. D, V. T. N.; Venkitanarayanan, K.; Kollanoor Johny, A., Antibiotic-Resistant Salmonella in the Food Supply and the Potential Role of Antibiotic Alternatives for Control. *Foods (Basel, Switzerland)* **2018,** 7, (10).
4. Thomassen, G. M. B.; Reiche, T.; Tennfjord, C. E.; Mehli, L., Antibiotic Resistance Properties among Pseudomonas spp. Associated with Salmon Processing Environments. *Microorganisms* **2022,** 10, (7).
5. Griffin, M. O.; Fricovsky, E.; Ceballos, G.; Villarre, F., Tetracyclines: a pleitropic family of compounds with promising therapeutic properties. Review of the literature. *American Journal of Physiology-Cell Physiology* **2010,** 299, (3), C539-C548.
6. Conforti, C.; Giuffrida, R.; Zalaudek, I.; Di Meo, N., Doxycycline, a widely used antibiotic in dermatology with a possible anti-inflammatory action against IL-6 in COVID-19 outbreak. *Dermatologic therapy* **2020,** 33, (4).
7. Dhar, R.; Kirkpatrick, J.; Gilbert, L.; Khanna, A.; Modi, M. M.; Chawla, R. K.; Dalal, S.; Maturu, V. N.; Stern, M.; Keppler, O. T., Doxycycline for the prevention of progression of COVID-19 to severe disease requiring intensive care unit (ICU) admission: A randomized, controlled, open-label, parallel group trial (DOXPREVENT. ICU). *PLoS One* **2023,** 18, (1), e0280745.
8. Butler, C. C.; Yu, L.-M.; Dorward, J.; Gbinigie, O.; Hayward, G.; Saville, B. R.; Van Hecke, O.; Berry, N.; Detry, M. A.; Saunders, C.; Fitzgerald, M.; Harris, V.; Djukanovic, R.; Gadola, S.; Kirkpatrick, J.; de Lusignan, S.; Ogburn, E.; Evans, P. H.; Thomas, N. P. B.; Patel, M. G.; Hobbs, F. D. R., Doxycycline for community treatment of suspected COVID-19 in people at high risk of adverse outcomes in the UK (PRINCIPLE): a randomised, controlled, open-label, adaptive platform trial. *The Lancet Respiratory Medicine* **2021,** 9, (9), 1010-1020.
9. Dorobisz, K.; Dorobisz, T.; Janczak, D.; Zatoński, T., Doxycycline in the coronavirus disease 2019 therapy. *Therapeutics and Clinical Risk Management* **2021**, 1023-1026.
10. Stec, J.; Kosikowska, U.; Mendrycka, M.; Stępień-Pyśniak, D.; Niedźwiedzka-Rystwej, P.; Bębnowska, D.; Hrynkiewicz, R.; Ziętara-Wysocka, J.; Grywalska, E., Opportunistic Pathogens of Recreational Waters with Emphasis on Antimicrobial Resistance—A Possible Subject of Human Health Concern. *International Journal of Environmental Research and Public Health* **2022,** 19, (12), 7308.
11. Chahal, C.; van den Akker, B.; Young, F.; Franco, C.; Blackbeard, J.; Monis, P., Pathogen and Particle Associations in Wastewater: Significance and Implications for Treatment and Disinfection Processes. *Advances in applied microbiology* **2016,** 97, 63-119.
12. Mateo-Sagasta, J.; Zadeh, S. M.; Turral, H.; Burke, J., Water pollution from agriculture: a global review. Executive summary. **2017**.
13. Toze, R., Microbial pathogens in wastewater: literature review for urban water systems multi-divisional research program. **1997**.
14. Qin, S.; Xiao, W.; Zhou, C.; Pu, Q.; Deng, X.; Lan, L.; Liang, H.; Song, X.; Wu, M., Pseudomonas aeruginosa: pathogenesis, virulence factors, antibiotic resistance, interaction with host, technology advances and emerging therapeutics. *Signal Transduction and Targeted Therapy* **2022,** 7, (1), 199.
15. Mena, K. D.; Gerba, C. P., Risk assessment of Pseudomonas aeruginosa in water. *Reviews of environmental contamination and toxicology Vol 201* **2009**, 71-115.
16. Moradali, M. F.; Ghods, S.; Rehm, B. H., Pseudomonas aeruginosa lifestyle: a paradigm for adaptation, survival, and persistence. *Frontiers in cellular and infection microbiology* **2017,** 7, 39.
17. Tuon, F. F.; Dantas, L. R.; Suss, P. H.; Tasca Ribeiro, V. S., Pathogenesis of the Pseudomonas aeruginosa biofilm: A review. *Pathogens* **2022,** 11, (3), 300.

18. Pachori, P.; Gothalwal, R.; Gandhi, P., Emergence of antibiotic resistance Pseudomonas aeruginosa in intensive care unit; a critical review. *Genes & diseases* **2019,** 6, (2), 109-119.
19. Tong, C.; Hu, H.; Chen, G.; Li, Z.; Li, A.; Zhang, J., Disinfectant resistance in bacteria: Mechanisms, spread, and resolution strategies. *Environmental research* **2021,** 195, 110897.
20. Assadi, A. A.; Karoui, S.; Trabelsi, K.; Hajjaji, A.; Elfalleh, W.; Ghorbal, A.; Maghzaoui, M.; Assadi, A. A., Synthesis and Characterization of TiO(2) Nanotubes (TiO(2)-NTs) with Ag Silver Nanoparticles (Ag-NPs): Photocatalytic Performance for Wastewater Treatment under Visible Light. *Materials (Basel, Switzerland)* **2022,** 15, (4).
21. Mîndroiu, V. M.; Stoian, A. B.; Irodia, R.; Trușcă, R.; Vasile, E., Titanium Dioxide Thin Films Produced on FTO Substrate Using the Sol–Gel Process: The Effect of the Dispersant on Optical, Surface and Electrochemical Features. *Materials* **2023,** 16, (8), 3147.
22. Sihor, M.; Gowrisankaran, S.; Martaus, A.; Motola, M.; Mailhot, G.; Brigante, M.; Monfort, O., Anodic TiO2 Nanotube Layers for Wastewater and Air Treatments: Assessment of Performance Using Sulfamethoxazole Degradation and N2O Reduction. *Molecules (Basel, Switzerland)* **2022,** 27, (24), 8959.
23. Razali, M. H.; Ismail, N. A.; Yusoff, M. In *Study on Band Gap Energy of F Doped TiO2 Nanotubes*, Materials Science Forum, 2017; Trans Tech Publ: pp 234-238.
24. Khairy, M.; Zakaria, W., Effect of metal-doping of TiO2 nanoparticles on their photocatalytic activities toward removal of organic dyes. *Egyptian Journal of Petroleum* **2014,** 23, (4), 419-426.
25. Subramanian, M.; Vijayalakshmi, S.; Venkataraj, S.; Jayavel, R., Effect of cobalt doping on the structural and optical properties of TiO2 films prepared by sol–gel process. *Thin Solid Films* **2008,** 516, (12), 3776-3782.
26. Hosseini-Zori, M., Co-doped TiO2 nanostructures as a strong antibacterial agent and self-cleaning cover: synthesis, characterization and investigation of photocatalytic activity under UV irradiation. *Journal of Photochemistry and Photobiology B: Biology* **2018,** 178, 512-520.
27. Kim, C.; Kim, S.; Choi, J.; Lee, J.; Kang, J. S.; Sung, Y.-E.; Lee, J.; Choi, W.; Yoon, J., Blue TiO2 Nanotube Array as an Oxidant Generating Novel Anode Material Fabricated by Simple Cathodic Polarization. *Electrochimica Acta* **2014,** 141, 113-119.
28. Liu, C.; Wang, F.; Qiu, Y.; Liang, Q.; Mitsuzak, N.; Chen, Z., Facile electrodeposition of cobalt hydroxide on anodic TiO2 nanotubes arrays for enhanced photoelectrochemical application. *Journal of Photochemistry and Photobiology A: Chemistry* **2018,** 353, 200-205.
29. Satulu, V.; Mitu, B.; Ion, V.; Marascu, V.; Matei, E.; Stancu, C.; Dinescu, G., Combining Fluorinated Polymers with Ag Nanoparticles as a Route to Enhance Optical Properties of Composite Materials. *Polymers* **2020,** 12, (8), 1640.
30. Ansari, M.; Khan, H. M.; Khan, A. A., Evaluation of antibacterial activity of silver nanoparticles against MSSA and MRSA on isolates from skin infections. *Biology and medicine* **2011,** 3, 141-146.
31. Berdini, F.; Otalvaro, J. O.; Avena, M.; Brigante, M., Photodegradation of doxycycline in water induced by TiO2-MCM-41. Kinetics, TOC evolution and reusability. *Results in Engineering* **2022,** 16, 100765.
32. Seelandt, B.; Wark, M., Electrodeposited Prussian Blue in mesoporous TiO2 as electrochromic hybrid material. *Microporous and Mesoporous Materials* **2012,** 164, 67-70.
33. Liu, Z.; Zhang, Q.; Qin, L.-C., Reduction in the electronic band gap of titanium oxide nanotubes. *Solid state communications* **2007,** 141, (3), 168-171.
34. Mîndroiu, V. M.; Stoian, A. B.; Irodia, R.; Trușcă, R.; Vasile, E., Titanium Dioxide Thin Films Produced on FTO Substrate Using the Sol–Gel Process: The Effect of the Dispersant on Optical, Surface and Electrochemical Features. *Materials* **2023,** 16, (8), 3147.
35. Derbali, A.; Attaf, A.; Saidi, H.; Benamra, H.; Nouadji, M.; Aida, M. S.; Attaf, N.; Ezzaouia, H., Investigation of structural, optical and electrical properties of ZnS thin films prepared by ultrasonic spray technique for photovoltaic applications. *Optik* **2018,** 154, 286-293.
36. Choudhury, B.; Choudhury, A., Oxygen defect dependent variation of band gap, Urbach energy and luminescence property of anatase, anatase–rutile mixed phase and of rutile phases of TiO2 nanoparticles. *Physica E: Low-dimensional Systems and Nanostructures* **2014,** 56, 364-371.
37. Attaf, A.; Derbali, A.; Saidi, H.; Benamra, H.; Aida, M. S.; Attaf, N.; Ezzaouia, H.; Derbali, L., Physical properties of Pb doped ZnS thin films prepared by ultrasonic spray technique. *Physics Letters A* **2020,** 384, (26), 126199.
38. Bilek, O.; Fialova, T.; Otahal, A.; Adam, V.; Smerkova, K.; Fohlerova, Z., Antibacterial activity of AgNPs-TiO(2) nanotubes: influence of different nanoparticle stabilizers. *Rsc Adv* **2020,** 10, (72), 44601-44610.

39. Gelderman, K.; Lee, L.; Donne, S., Flat-Band Potential of a Semiconductor: Using the Mott Schottky Equation. *Journal of Chemical Education - J CHEM EDUC* **2007,** 84.
40. Wang, S.; Pan, L.; Song, J.-J.; Mi, W.; Zou, J.-J.; Wang, L.; Zhang, X., Titanium-Defected Undoped Anatase TiO2 with p-Type Conductivity, Room-Temperature Ferromagnetism, and Remarkable Photocatalytic Performance. *Journal of the American Chemical Society* **2015,** 137, (8), 2975-2983.
41. Sang, L.; Tan, H.; Zhang, X.; Wu, Y.; Ma, C.; Burda, C., Effect of Quantum Dot Deposition on the Interfacial Flatband Potential, Depletion Layer in TiO 2 Nanotube Electrodes, and Resulting H 2 Generation Rates. 2012; Vol. 116.
42. Cánovas, R.; Sleegers, N.; van Nuijs, A. L.; De Wael, K., Tetracycline antibiotics: elucidating the electrochemical fingerprint and oxidation pathway. *Chemosensors* **2021,** 9, (7), 187.
43. Bahrudin, N. N., Evaluation of degradation kinetic and photostability of immobilized TiO2/activated carbon bilayer photocatalyst for phenol removal. *Applied Surface Science Advances* **2022,** 7, 100208.
44. Rani, S.; Garg, A.; Singh, N., Efficient degradation of doxycycline and ofloxacin in an aqueous environment using Fe and Cu doped TiO 2-SiO 2 photocatalyst under sunlight. *Environmental Engineering Research* **2022,** 27, (4).
45. Li, Q.; Jiang, L.; Li, Y.; Wang, X.; Zhao, L.; Huang, P.; Chen, D.; Wang, J., Enhancement of Visible-Light Photocatalytic Degradation of Tetracycline by Co-Doped TiO2 Templated by Waste Tobacco Stem Silk. *Molecules (Basel, Switzerland)* **2023,** 28, (1), 386.